A Classical and Ab Initio Study of the Interaction of the Myosin Triphosphate Binding Domain with ATP

Todd J. Minehardt,* Nicola Marzari,* Roger Cooke,† Edward Pate,‡ Peter A. Kollman,§ and Roberto Car*

*Department of Chemistry, Princeton University, Princeton, New Jersey 08544; †Department of Biochemistry and Biophysics and the Cardiovascular Research Institute, University of California, San Francisco, California 94143; ‡Department of Pure and Applied Mathematics, Washington State University, Pullman, Washington 99164; and §Department of Pharmaceutical Chemistry, University of California, San Francisco, California 94143 USA

ABSTRACT We used classical molecular mechanics (MM) simulations and quantum mechanical (QM) structural relaxations to examine the active site of myosin when bound to ATP. Two conformations of myosin have been determined by x-ray crystallography. In one, there is no direct interaction between switch 2 and the nucleotide (open state). In the other (closed state), the universally conserved switch 2 glycine forms a hydrogen bond with a γ-phosphate oxygen. MM simulations indicate that the two states are thermodynamically stable and allow us to investigate the extent to which the P-loop, switch 1, and switch 2 are involved in hydrolysis. We find that the open structure has a higher affinity for ATP than the closed structure, and that ATP is distorted toward a transition state by interactions with the protein. We also examine how the structure of the binding site changes with either MgATP or CaATP as the nucleotide in myosin in the open conformer. Our analyses suggest that higher CaATPase rates occur because the leaving phosphate (P_i) group is more weakly bound and dissociation occurs faster. Finally, we validate the use of a particular formulation of a QM methodology (Car-Parrinello) to further refine the structures of the active site.

INTRODUCTION

The motor protein myosin uses the free energy provided by the hydrolysis of ATP to generate biological force and motion. Protein-nucleotide interactions give rise to conformational changes in the protein that result in the production of work. Despite concerted efforts to elucidate how the chemical free energy is harnessed, amplified, and transferred from the nucleotide binding site to the portion of the protein that functions as the working motor element, this process remains largely unresolved. Additional understanding of the protein-nucleotide interaction is necessary to resolve the interaction, and is the goal we pursue here.

X-ray crystallographic solutions of the motor domain of myosin (Smith and Rayment, 1996a; Fisher et al., 1995; Gulick et al., 1997, 2000; Dominguez et al., 1998; Houdusse et al., 1999) show considerable structural and functional homology with both kinesin-family motors (Kull et al., 1996; Sablin et al., 1996, 1998; Gulick et al., 1998; Kozielski et al., 1997; Müller et al., 1999) and with the guanosine nucleotide binding proteins (reviewed in Vale, 1996; Kull et al., 1998). The structural homology is particularly striking at the triphosphate binding domain of the nucleotide site. It is composed of three highly conserved elements: switch 1, switch 2, and the P-loop, Walker A motif (Walker et al., 1982) found in most, but not all, ATPases. The switch notation derives from the original identification of these structural elements in the G-proteins.

In all myosin x-ray structures these three elements form the P_i-tube, a narrow channel into which the nucleotide triphosphates bind and hydrolysis subsequently occurs (Yount et al., 1995). The x-ray structures show extensive coordination between the nucleotide and the P-loop, switches 1 and 2, and the magnesium ion. A comparison of the motor domain of *Dictyostelium discoideum* (Dd) myosin in the Dd S1 · MgADP · BeF_x state with that in the Dd S1 · MgADP · AlF_4^- (Fisher et al., 1995) or Dd S1 · MgADP · VO_4 state (Smith and Rayment, 1996b) provided the first suggestions as to how coordination changes at the nucleotide site associated with the hydrolysis step could result in motility. Exhibiting trigonal, bipyramidal geometry for the fluorine or oxygen atoms at the γ-phosphate position, the latter two states are thought to mimic the nucleotide hydrolysis state intermediate. In relation to the Dd S1 · MgADP · BeF_x state, the Dd S1 · MgADP · AlF_4^- and Dd S1 · MgADP · VO_4 states show a dramatic repositioning of switch 2 and adjacent switch 2 α-helix (also termed the relay helix). This displacement has been suggested to be stabilized by two coordinations lacking in the Dd S1 · MgADP · BeF_x state (Fisher et al., 1995; Smith and Rayment, 1996a; reviewed in Holmes, 1996; Cooke, 1997). One is a hydrogen bond from the universally conserved glycine in switch 2 to a γ-phosphate position fluorine or oxygen. The other is a salt bridge between conserved residues in switch 1 and switch 2. A popular hypothesis is that myosin-based motility results from the propagation of these conformational changes to the myosin neck via the converter domain (Fig. 1) (Fisher et al., 1995; Smith and Rayment, 1996a; reviewed in Holmes, 1996; Cooke, 1997).

Submitted July 9, 2001, and accepted for publication October 19, 2001.

Address reprint requests to Dr. Todd J. Minehardt, Dept. of Chemistry, Princeton University, Princeton, NJ 08544. Tel.: 609-258-1932; Fax: 609-258-6746; E-mail: tjm@princeton.edu.

Nicola Marzari's present address is Dept. of Materials Science and Engineering, Massachusetts Institute of Technology, Cambridge, MA 02139.

0006-3495/02/02/660/16 $2.00

FIGURE 1 Ribbon diagram of the Ch_{giz} structure (PDB 1BR4) in the region of the active site. The nucleotide, MgATP, is visible in the upper left corner and is colored as follows: nitrogen is purple, carbon is gray, oxygen is red, phosphorus is yellow, and Mg^{2+} is the green sphere. The orange-colored P-loop lies just to the upper right of the nucleotide in this view (aa 179-186 in Dd S1 and 177-184 in Ch_{giz} S1). Switch 1 is magenta (aa 233-238 in Dd S1 and 242-247 in Ch_{giz} S1). Switch 2 is dark green (aa 454-459 in Dd S1 and 465-470 in Ch_{giz} S1). The universally conserved glycine residue (Gly-457 in Dd S1 and Gly-468 in Ch_{giz} S1) is represented in a ball-and-stick fashion to emphasize how close this moiety is to the γ-phosphate of ATP in Ch_{giz} S1. In the open-switch 2 conformation of Dd S1, it is 4 Å more distant (not shown). The switch 2 motif is separated from the switch 2 α-helix (aa 462-494 in Dd S1 and 478-508 in Ch_{giz} S1), shown in blue, by 7-aa residues, which are rendered in pink. The yellow and purple α-helices are part of the converter domain. Conformational changes arising at the active site due to changes in the coordination between switch 2 and the nucleotide are hypothesized to be propagated to the converter region via the switch 2 α-helix. Rotation of the converter region is then postulated to cause the neck (not shown) to function as a rowing oar.

Other coordination changes at the nucleotide site are seen, however. Additionally, the structure of chicken gizzard (Ch_{giz}) S1 bound to the MgATP analog, MgADP · BeF_x (Dominguez et al., 1998), shows a similar switch 2 movement as in the Dd S1 · MgADP · AlF_4^- and Dd S1 · MgADP · VO_4 states in the absence of the hydrolysis transition state intermediate. Other factors can also dramatically perturb the relationship between conformational changes at the nucleotide site and motor function. For example, MgATP is the physiological substrate and the x-ray structures show Mg^{2+} chelating to the β- and γ-phosphate positions of ATP^{4-}. Substituting Ca^{2+} for Mg^{2+} dramatically elevates the myosin ATPase rate, while slightly inhibiting the actomyosin ATPase rate and dramatically down-regulating skinned fiber sliding velocity (Polosukhina et al., 2000). Even more perplexing are uncouplers such as PrNANTP (Pate et al., 1991) and DNPhAPrTP (Wang et al., 1993), which are rapidly hydrolyzed by both myosin and actomyosin but do not support motility. These nucleotide analogs would suggest that conformational changes at the γ-phosphate position associated with hydrolysis as suggested by the crystal structures may be necessary, but are not sufficient for motility. All these factors call into question the precise relationship between hydrolysis intermediates, switch movements, and ultimately, motility. Clearly, additional information is required to determine the correct relationships.

A limitation of a crystal structure is that it is a static picture of a single conformation of a protein, obtained in the presence of crystal contact packing forces, and generally under nonphysiological conditions. As noted above, this can confound interpretation. What is desired is to augment the insights obtained from x-ray crystallography with nonstatic analyses. In this regard, classical molecular mechanics (MM) offers us an extremely powerful tool for analyzing the structural, mechanistic, and energetic properties of biomolecules. Given the atom locations from a crystal structure, one can obtain detailed descriptions of how certain parts of the protein move with respect to time, simulating solvated, physiological conditions.

For all the power of MM, there remains a shortcoming. The potential energy function used in these simulations is bound and thus does not allow for the breaking or formation of chemical bonds any stronger than hydrogen and ionic bonds. We are therefore unable to "do chemistry" in the event that a reaction takes place. In most cases, such as when refining crystal structures or predicting conformations different from those observed in experiments, this limitation is not an impairment. However, when covalent reactions are considered, we must turn to quantum mechanical (QM) prescriptions.

QM simulations are inherently unbiased and can accurately describe bond-breaking reactions. The use of density-functional theory (Parr and Yang, 1989) in the generalized-gradient approximation to the exchange-correlation functional of Perdew et al. (1996, 1997) combines the merit of very high structural and thermodynamical accuracy with favorable scaling in the system size. This allows us to easily manage structures containing hundred of atoms. The electronic ground state can be determined using the Car-Parrinello (CP) approach (Car and Parrinello, 1985) allowing for very efficient structural optimizations and the ability to evolve the electronic ground state "on-the-fly." The electrons adiabatically follow the ionic motion, thus allowing true first-principle molecular dynamics simulations, without resorting to any force field parametrization. CP was originally developed within the solid-state physics community

and applied to systems of interest to those scientists. In recent years, however, there have been many applications of this technique to systems of biological relevance (Alber et al., 1999a, b; Alber and Carloni, 2000; Pantano et al., 2000; Piana and Carloni, 2000; Rothlisberger et al., 2000; Sulpizi and Carloni, 2000; Cecconi et al., 2001; Dal Peraro et al., 2001). We have the capability to use this technology to investigate the complex chemical and physical behavior of reactive systems such as the one studied herein.

The x-ray crystal structures of Dd S1 · MgADP · BeF_x myosin and Ch_{giz} S1 · MgADP · BeF_x are thought to represent the motor in the open-switch 2 prehydrolysis state and the closed-switch 2 transition state, respectively. As noted, however, ambiguities remain in relating structurally observed conformational changes at the nucleotide site to the motor cycle. Here we use MM analyses of these two structures to examine the stability of these structures, the energetics of nucleotide binding, the coordination of the P-loop and switch regions to each other and the nucleotide, and the effects of the nucleotide-chelated metal to better comprehend the relationship among the x-ray structures, nucleotide hydrolysis, and motility. We choose to analyze these two structures (one with an open switch 2, the other closed) because they both contain the same nucleotide, which we modeled with ATP. The analyses suggest that certain amino acid residues at the nucleotide site have crucial roles in hydrolysis. We extend the analyses through the use of CP structural relaxations to better refine the geometries of these residues at the active sites to better understand their involvement in the chemical reaction of hydrolysis.

METHODS

Classical molecular dynamics

The structures for Dd S1 · MgADP · BeF_x (Protein Data Bank 1MMD) and Ch_{giz} S1 · MgADP · BeF_x (Protein Data Bank 1BR4) were obtained and subsequently first refined with classical MM methods. In both cases, BeF_3 was replaced with the γ-phosphate group. Because we were interested only in the motor domain fragment containing the nucleotide binding site, we truncated the Ch_{giz} S1 · MgADP · BeF_x structure to include the first 705 amino acid (aa) residues of heavy chain A; the Dd S1 · MgADP · BeF_x x-ray structure contained 743 aa residues. We note that although the Dd and Ch_{giz} structures are similar in size, they are not identical. However, what differences do exist are relegated to structural features far removed from the active site and surrounding domains of interest. For the CaATP simulations we used the Dd S1 · MgADP · BeF_x structure and replaced Mg^{2+} with Ca^{2+}.

The AMBER 6.0 package (Case et al., 1999; Pearlman et al., 1995) and the force field of Cornell et al. (1995) were used for these calculations. Charges for ATP were computed by first performing a single-point energy calculation on the molecule (the geometry of the nucleotide as determined in the Dd S1 · MgADP · BeF_x structure was used) at the Hartree-Fock level of theory. A 6-31G* basis was used and the RESP algorithm (Bayly et al., 1993) was then used to fit the electrostatic potential to the molecule and determine atom-centered charges. Parameters for Ca^{2+} were taken from Aqvist (1992). For Mg^{2+}, the parameters were the same as in an earlier study on ncd (Minehardt et al., 2001). Using the *tLEaP* module of AMBER 6.0, we added hydrogen atoms and protonated all histidine residues at the δ position. Na^+ counterions were added to produce an overall electrically neutral system.

A box of TIP3P waters (Jorgensen et al., 1983) was then used to solvate the system, leaving a 10 Å border between the edges of the box and the closest atoms of the protein. All crystallographic waters in the Dd S1 · MgADP · BeF_x structure were first removed before the solvation step. Importantly, as discussed in Results, the MM simulations subsequently accurately reproduced the locations of the crystallographic waters adjacent to the nucleotide triphosphates in the P_i-tube, thus providing additional confidence in our simulations. Only two P_i-tube crystallographic waters interacting with the nucleotide were resolved in the Ch_{giz} S1 · MgADP · BeF_x x-ray structure, compared with seven in the Dd S1 · MgADP · BeF_x structure. Preliminary MM simulations indicated that if these waters were removed, the nucleotide would not be properly solvated due to the fact that switch 2 was displaced closer to the nucleotide, closing off the P_i-tube, and therefore precluding mobile waters from entering the region adjacent to the nucleotide during the MM simulations. These two waters, but no others, were retained for the simulations.

The simulations were completed in two steps. In the first, the entire system (94,257 atoms for Dd S1 · MgATP, 94,260 for Dd S1 · CaATP, and 127,370 atoms for Ch_{giz} S1) was energy-minimized using the *SANDER* module of AMBER 6.0. The steepest descent algorithm was used for the first 10 cycles, after which the conjugate gradient method was utilized until a total of 1000 cycles were completed. The minimized system was then heated to 300 K for 500 ps using the temperature scaling scheme of Berendsen et al. (1984). Periodic boundary conditions were used and conditions were kept at constant pressure. The SHAKE algorithm (Ryckaert et al., 1977) was used at every step of the simulations and allowed us to use a 2-fs time step. On 16 processors of our SGI Origin 2000 (R12000, 300MHz CPUs), the MM runs took 115 and 155 h for the Dd and Ch_{giz} systems, respectively.

MM-PBSA energetics calculations

To assess how significant the displacement of switch 2 was in terms of binding, we completed free energy calculations for MgATP as the nucleotide and either Dd or Ch_{giz} S1 as the receptor. The free energies of binding of the nucleotide to the enzyme were calculated as in a previous study on ncd (Minehardt et al., 2001). In short, we used the scheme of Srinivasan et al. (1998) and Massova and Kollman (1999), where snapshots from the MM simulations, here representing 4 ps in time, were evaluated to yield the average molecular mechanical energies, $\langle E_{MM} \rangle$, the sum of the average nonpolar and polar solvation (Poisson-Boltzmann surface area, PBSA) energies (Osapay et al., 1996; Bashford et al., 1997; Demchuk et al., 1997; Yang and Honig, 1995a, b; Yang et al., 1996; Smith and Honig, 1994; Honig et al., 1993), $\langle G_{PBSA} \rangle$, and the entropic term, $-T\langle S_{MM} \rangle$. The $\langle E_{MM} \rangle$ term was itself an average of the electrostatic, van der Waals, and internal energies and was computed using the *anal* package of AMBER 6.0 (Case et al., 1999). The polar solvation term was calculated by solving the nonlinear Poisson-Boltzmann equation (Sharp and Honig, 1990); the solvent-accessible surface area (SASA) algorithm due to Sanner et al. (1996) was used to compute the nonpolar contribution to $\langle G_{PBSA} \rangle$. The entropic contribution to the binding energy, $-T\langle S_{MM} \rangle$, was difficult to compute due to the size of the systems considered in this study. However, it has been estimated to be ~+20 kcal/mol for the binding of ligands similar in size to ATP (Massova and Kollman, 1999; Chong et al., 1999). This value was also seen to be appropriate in a study of ATP binding to kinesin-family motors (Minehardt et al., 2001) and was used here.

Car-Parrinello structural relaxations

Three truncated structures of the active site were considered, each taken from energy-minimized spatially averaged MM structures from the last 10 ps of simulation. For the Dd S1 · MgATP active site we included Ser-181–

TABLE 1 Average RMS deviations (in angstroms) of the C_α backbone (first four entries) and nucleotide (including the metal cation) atoms

	Dd S1 · MgATP	Dd S1 · CaATP	Ch S1 · MgATP
Switch 1	0.38 (0.06) [0.20:0.60]	0.32 (0.08) [0.15:0.55]	0.42 (0.10) [0.17:0.73]
Switch 2	0.44 (0.09) [0.11:0.70]	0.74 (0.10) [0.24:1.10]	0.32 (0.08) [0.08:0.60]
Switch 2 α-helix	0.91 (0.17) [0.37:1.40]	0.74 (0.14) [0.40:1.30]	1.15 (0.21) [0.55:1.64]
P-loop	0.24 (0.06) [0.09:0.53]	0.32 (0.06) [0.13:0.51]	0.30 (0.08) [0.13:0.60]
Nucleotide	0.35 (0.06) [0.18:0.54]	0.39 (0.16) [0.15:0.84]	0.46 (0.06) [0.16:0.63]

RMS deviations (σ) (range in brackets) are measured over 500 ps of MM simulation and are referenced against the minimized crystal structure.

Glu-187 in the P-loop, Asn-233 and Asn-235–Ser-237 in switch 1, and Asp-454 in switch 2. Ser-181 and Asn-235 were terminated with NH_2 groups; Asp-454 was modeled as $CH_3CH_2COO^-$; Asn-233 was modeled as $CH_3CH_2CONH_2$; Glu-187 was terminated with a COOH group; and Ser-237 was terminated with an aldehyde, CHO; the nucleotide was terminated at N^9 (where the ribose joins the adenine moiety). This nitrogen was saturated and became an NH_2 group. Including four waters and the cation, the resulting structure contained 194 atoms. We used an orthorhombic cell of dimension (a.u.) $38 \times 37 \times 42$, which included a 10 a.u. buffer to insulate copies of the system in the periodic boundary conditions.

When CaATP was considered, 193 atoms were included: Ser-181–Glu-187 (terminated with hydrogens) from the P-loop, Asn-233 (modeled as $CH_3CH_2CONH_2$) and Asn-235–Ser-237 (terminated with hydrogens) from switch 1, Asp-454 (modeled as $CH_3CH_2COO^-$) and Ser-456 (modeled as CH_3CH_2OH) from switch 2, the nucleotide (as above), the metal ion, and three waters identified by the MM simulation. The active site from Ch_{giz} (186 atoms) was chosen as for Dd S1 · MgATP, using the homologous amino acids, with the following exceptions: the C- and N-termini were capped with hydrogens; Gly-468 (homologous to Gly-457 in Dd S1) was included and modeled as CH_3NH_2; and only two waters were included that were present in the P_i-tube (AMBER simulations and crystal structure). Note that, unlike the Dd S1 · MgATP active site, the Dd S1 · CaATP and Ch_{giz} active sites did not include the backbone oxygen of Ser-237 because there is no crystallographic or computational (MM) evidence that this atom is part of the hydrogen bond network present in that region of the myosin-nucleotide complex. Additionally, although the x-ray crystal structure of Dd Mg (Fisher et al., 1995) suggested that Arg-238 helps stabilize the lytic water via a weak interaction (3.4 Å, N–O distance), our MM simulations did not confirm this (the distance grows to 4.6 Å during the course of the simulation of Dd Mg) and therefore we did not include this residue in any of the three models. A cubic cell (38 a.u. on a side) was sufficient for this system, and as previously noted, it included the 10 a.u. buffer region.

For all CP simulations, Vanderbilt ultrasoft pseudopotentials (Vanderbilt, 1990) were used and enabled the use of a 25 Ry cutoff for the basis set. We used the PBE exchange-correlation potential (Perdew et al., 1996, 1997) and the in-house version of the Car-Parrinello code, CP90, maintained by our group at Princeton University. Starting with the structures as determined above, we first performed 50 electronic minimization steps ($\Delta t = 5$ a.u.) to converge to a realistic representation of the ground state wavefunction for the system. In the next phase, we refined the electronic wavefunction for 500 minimization steps using the same Δt. Finally, ions and electrons were allowed to move and the system was minimized for 1000 steps with $\Delta t = 10$ a.u. On 16 SMP Power3-II processors on our IBM SP Winterhawk-2, each system was minimized in ~72 h.

RESULTS

Two x-ray structures of myosin complexed with the identical bound ATP analog, ADP · BeF_x, are available. However, there is a major difference between the two structures at the nucleotide site. In one (Dd), switch 2 is in the open conformation. In the other structure (Ch_{giz}), switch 2 is in the closed conformation. We now use MM simulations on the fully solvated proteins with differing metals chelated to the nucleotide to better understand the implications of these structural differences. For brevity, we will refer to the Ch_{giz} S1 · MgATP structure as Ch_{giz}, the Dd S1 · MgATP structure as Dd Mg, and the Dd S1 · CaATP structure as Dd Ca. The classical molecular mechanical simulations are abbreviated as MM, and the Car-Parrinello simulations as CP.

Stability of the modeled structures

We first examined the stability of protein structures. The MM simulations showed that the structures were temporally stable following an initial, ~50 ps, equilibration period. In Table 1 we summarize the RMS deviations of the C_α backbone of switch 1, switch 2, the switch 2 α-helix, the P-loop, and the nucleotide (standard deviations and the range are also included). In all cases, the structure to which the evolving system was compared was the energy-minimized structure that resulted from the first step of the MM simulation process. The latter step was performed to eliminate bad crystal contacts.

For Dd Mg, Dd Ca, and Ch_{giz}, the RMS deviations of switch 1, the P-loop, and the nucleotide are virtually indistinguishable. The values fall within the range of 0.24–0.46 Å, indicating that these structural features are very stable and probably represent local minima on the global free energy surface. Switch 1 is very stable in the observed, closed, conformation and exhibits almost identical RMS deviations for both Dd and Ch_{giz}. The same can be said for the P-loop, which is commonly believed not to undergo any conformational change during binding and subsequent nucleotide hydrolysis. Recalling that we modeled the CaATP structure by replacing Mg^{2+} with Ca^{2+} in the initial, crystal structure of Dd myosin, it is reasonable to assume that an initial equilibration period would also be required with the different metal. In Fig. 2 a plot of the RMS deviation of CaATP is shown and exhibits exactly the predicted behavior. After ~75 ps, the position of the nucleotide has stabilized. As reported in Table 1, the position of CaATP is about as stable as is MgATP in either the Dd or Ch_{giz} structure.

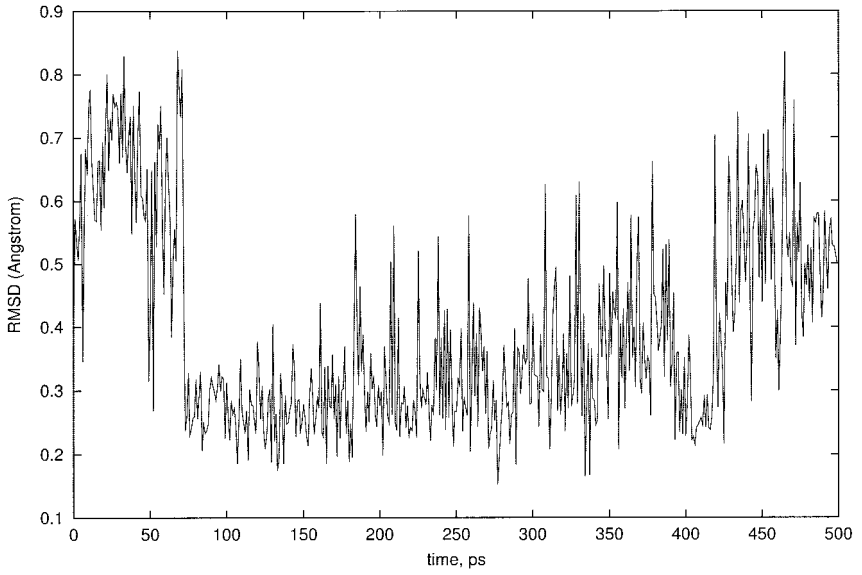

FIGURE 2 RMS deviation plot of the CaATP nucleotide in the Dd S1 structure. The structure to which the atomic positions are compared at each 1-ps time step (total time = 500 ps) is the minimized initial structure. The structures from the 500 time steps are from the MM run at 300 K.

The largest differences from the MM simulations appear in the relative stabilities of the switch 2 α-helix. In Fig. 3 the RMS deviation of the C_α backbone of the switch 2 α-helix in Ch_{giz} is plotted as a function of time. The plot for Dd Mg (not shown) is qualitatively similar, but displays almost one σ less movement than the average RMS deviation for the switch 2 α-helix in Ch_{giz} (Table 1). By contrast, the RMS deviation of the C_α backbone of the switch 2 is plotted in Fig. 4. Finally, we note that although the number of couplings between switch 2 and the nucleotide is greatest for Dd Ca, they apparently are not strong enough to stabilize both switch 2 and the switch 2 α-helix, because RMS deviations for these structural features are identical (Table 1).

Energetics of the Dd Mg and Ch_{giz} systems

The conformational change associated with the transition from the open to closed state of switch 2, and the attendant

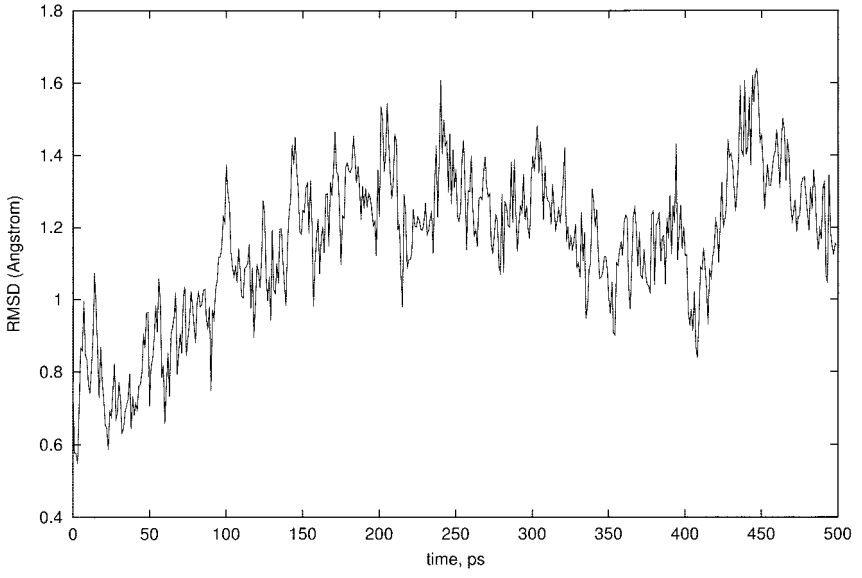

FIGURE 3 RMS deviation of the C_α backbone of the switch 2 α-helix in the Ch_{giz} S1 structure. The procedure for producing the plot is exactly the same as for Fig. 2.

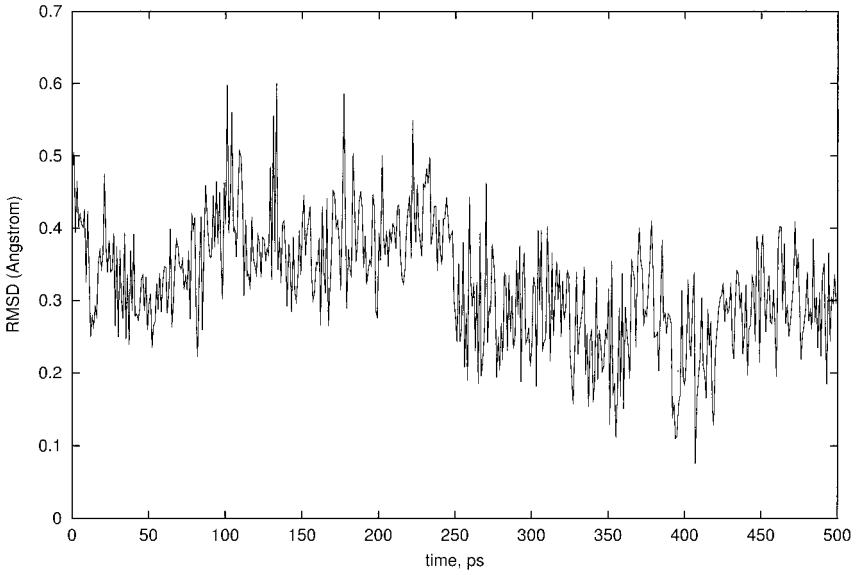

FIGURE 4 RMS deviation of the C_α backbone of switch 2 in the Ch_{giz} S1 structure. The procedure is described as for Fig. 2.

changes in the coordination to the triphosphate nucleotide, would be expected to alter the energies of the two systems and the binding energies of the substrate. We investigated this effect using the MM-PBSA method to determine binding energies. Table 2 presents the components of the energies of the two structures. The sizes of the two systems involved, along with fact that we are dealing with structures that have significant, but not complete sequence homology, introduced some variation into the calculations (Minehardt et al., 2001). Nonetheless, the calculations indicated that Dd S1 is a more favored receptor for MgATP than is Ch_{giz}. This assertion is supported by examining Table 3, where the components of the binding energies are presented. Estimating $-T\Delta S$ as $+20$ kcal/mol (Minehardt et al., 2001), and adding this to the enthalpies given in Table 3, we found that $\Delta G_{bind} = -16$ kcal/mol for the Dd S1 · MgATP system and $\Delta G_{bind} = 0$ kcal/mol for the Ch_{giz} · MgATP system. As suggested by the energetics reported in Table 2, we see that the Ch_{giz} structure interacted less favorably with the nucleotide than did the Dd Mg structure.

An explanation for the difference in binding energies is as follows. The Dd Mg structure was crystallized in the presence of an MgATP analog. Based on the position of switch 2 in the crystal structure, it represents a system *before* hydrolysis occurs. Thus it is reasonable that ΔG_{bind} should be negative; that is, the prehydrolysis conformer of S1 (not to be confused with pre and posthydrolysis and transition state conformers of the nucleotide) should significantly bind a prehydrolysis nucleotide. We also note that our value for this quantity agrees very nicely with the experimentally observed value of -18 kcal/mol (Taylor, 1979). The Ch_{giz} structure, although crystallized with the same MgATP analog, clearly is not in a conformation suggestive of the prehydrolysis step. Instead, the P_i-tube is more crowded than in the Dd structure due to a 4 Å displacement of switch 2 toward the nucleotide. There are also fewer waters present

TABLE 2 Energies (standard deviations) for the two S1 · MgATP structures

	Dd S1 · MgATP			Ch S1 · MgATP		
	Complex	Receptor	Ligand	Complex	Receptor	Ligand
$E_{electrostatic}$	−26280 (131)	−24600 (134)	−1286 (12)	−23770 (80)	−22200 (80)	−1272 (11)
E_{vdW}	−3370 (50)	−3365 (50)	41 (6)	−3170 (35)	−3162 (35)	40 (5)
$E_{internal}$	12510 (70)	12430 (70)	81 (7)	12110 (100)	12030 (100)	80 (6)
E_{MM}	−17140 (140)	−15540 (140)	−1165 (7)	−14831 (100)	−13330 (100)	−1152 (8)
$E_{nonpolar}$	180 (2)	182 (2)	4 (0.05)	190 (1)	191 (1)	4 (0.05)
E_{PB}	−10300 (150)	−10300 (150)	−400 (6)	−11800 (85)	−11740 (85)	−410 (6)
$E_{solvation}$	−10110 (150)	−10130 (147)	−400 (6)	−11600 (85)	−11550 (85)	−405 (6)
$E_{PB+electrostatic}$	−36575 (50)	−34910 (50)	−1685 (10)	−35580 (30)	−33940 (35)	−1680 (8)
$E_{total,PB}$	−27255 (60)	−25660 (60)	−1557 (5)	−26450 (80)	−24880 (80)	−1557 (4)

Quantities are in kcal/mol and standard deviations are in parentheses.
Twenty-five snapshots from the 400–500 ps segment of the MM runs were used for the data analyses presented in this table.

TABLE 3 Binding energies (standard deviations) for the two S1 · MgATP systems studied

	Dd S1 · MgATP	Ch S1 · MgATP
$E_{electrostatic}$	−395 (15)	−300 (17)
E_{vdW}	−47 (5)	−50 (5)
E_{gas}	−440 (15)	−350 (15)
$E_{nonpolar}$	−6 (0.5)	−5 (0.5)
E_{PB}	410 (12)	335 (15)
$E_{solvation}$	405 (12)	330 (15)
$E_{PB+electrostatic}$	17 (8)	36 (10)
$E_{total,PB}$	−36 (5)	−20 (8)

Quantities are in kcal/mol and standard deviations are in parentheses. Twenty-five snapshots from the 400–500 ps segment of the MM runs were used for the data analyses presented in this table.

than in the Dd, prehydrolysis, structure. This arrangement observed in Ch_{giz} suggests that the *protein* is in a conformation somewhere along the reaction pathway. That is, hydrolysis of the nucleotide is either in the process of occurring or has just taken place, and the surrounding protein has undergone the requisite structural changes in and around the hydrolysis site. Thus, the receptor—itself in a transition or posttransition state—would bind a transition state analog more favorably than a nucleotide in a prehydrolysis conformation. In short, the computed ΔG_{bind} value for the Ch_{giz} structure implies that the protein is expecting a nucleotide with a geometry more similar to a transition state intermediate than to MgATP with tetrahedrally coordinated oxygens at the γ-phosphate position: a prehydrolysis nucleotide state. It does not have a preference for binding or releasing this nucleotide.

Interactions of the nucleotide with the protein

Aside from the goals of understanding the structure and function of a complicated and important biophysical system such as myosin, we are also laying the foundation for future studies of the hydrolysis reaction itself. Thus, it is of extreme import that the CP method in general, and the Vanderbilt ultrasoft pseudopotentials and PBE exchange-correlation functional in particular, can be shown to produce results that not only agree with experimental studies and MM simulations, but provide additional information that would otherwise be unattainable. As noted in both Introduction and Methods, CP allows us to make and break chemical bonds. On a much more fundamental level, no parametrizations are used when computing the forces in a system, and thus our structural refinements ought to provide the most reliable data about said structures. Finally, the S1 · XATP (X is calcium or magnesium) active site warrants investigation by a method such as CP because simulation accuracy requires that the electronic degrees of freedom must be characterized explicitly in such a highly charged and reactive system.

In Figs. 5–7 we present the hydrogen bonding patterns from the CP structural relaxations for Dd Mg, Dd Ca, and Ch_{giz}, respectively. Please note that the numbering of the amino acid sequences in all three figures is that of Dd. This scheme was chosen to simplify comparisons between the Dd and Ch_{giz} figures and to simplify Results and Discussion of this study. Thus, when residues are numbered, they are numbered as in the Dd crystal structure. The corresponding numbers in Ch_{giz} are as follows: aa 242-247 for switch 1, aa 465-470 for switch 2, aa 177-184 for the P-loop, and aa 478-508 for the switch 2 α-helix. The reader is advised that the hydrogen bonding patterns for Dd S1 complexed with either MgADP·BeF_x (Fig. 6 in Fisher et al., 1995) or MgADP·VO_4 (Fig. 11 in Smith and Rayment, 1996a), as observed in the crystal structures, are also of help in understanding the following section.

The P-loop

The P-loop is a glycine-rich motif that contains a universally conserved lysine. The side chain of this particular aa (Lys-185) carries a formal charge of +1 and is thus considered likely to interact significantly with a negatively charged nucleotide such as ATP. In both the Dd and Ch_{giz} structures, two of the remaining residues (Ser-181 and Thr-186) in the P-loop contain polar side chains that enhance the magnitude of the interaction with the substrate. Finally, there is a glutamic acid (which carries a formal charge of −1) at the 187 position.

When we examine Lys-185 in the crystal structure of Dd Mg, N_ζ is predicted to be equidistant to the γ- and β-phosphate oxygens to which it forms hydrogen bonds. In the CP simulations of Dd Mg, the length of the hydrogen bond between H_ζ–O_γ is shorter than that from H'_ζ–O_β (1.52 vs. 1.78 Å; see Fig. 5). This bond is the second shortest hydrogen bond observed in the system and warrants consideration of Lys-185 acting as a general acid toward the base that is the γ-phosphate moiety. We note that this feature is not distinguishable in the crystal structure. In the Ch_{giz} structure (Fig. 7), where N_ζ of Lys-185 is shown to be on average 0.4 Å further from the γ- and β-phosphate oxygens of ATP, we see that the H_ζ–O_γ distance is now slightly *longer* than the H'_ζ–O_β distance. Given that the Ch_{giz} structure is thought to closely resemble the transition state, it is reasonable to expect Lys-185 to stabilize the remaining ADP group, while Gly-457 in switch 2 (discussed below) provides extra coordination to the γ-phosphate leaving group.

Bond distances for interactions of Ser-181 and Thr-186 to the nucleotide are accurately reproduced by both MM and CP calculations for the Dd Mg (Fig. 5) and the Ch_{giz} (Fig. 7) models. Ser-181 stabilizes the γ-phosphate with a H-bond of ~1.6 Å, while the hydroxyl oxygen of Thr-187 interacts with Mg^{2+} over a distance of slightly >2 Å. Glu-187 provides additional contact to MgATP via a bond from the backbone amide hydrogen to O_α. This H-bond is

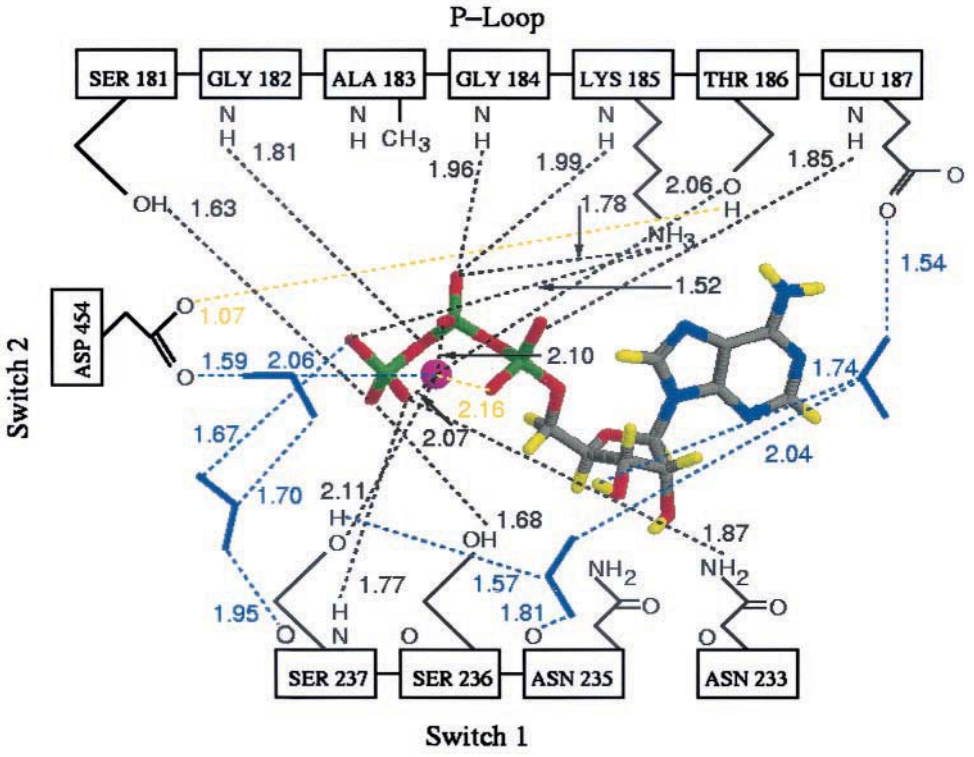

FIGURE 5 The hydrogen-bonding pattern from the final results of the CP simulations of the active site of Dd MgATP. Black lines represent H-bonds observed in the crystal structure (although hydrogens are not resolved by x-ray crystallography). Contacts involving the four water molecules present in the CP simulations are colored blue, although (with the exception of hydrogen to oxygen interactions) many of these contacts are also seen in the crystal structure, especially the water that bridges Asp-454 in switch 2 and Mg^{2+}. Finally, yellow lines indicate contacts that are not observed in the x-ray structure. For the nucleotide, the color scheme is as follows: hydrogen is yellow, carbon is gray, nitrogen is blue, oxygen is red, and phosphorus is green. The magenta sphere is the magnesium cation.

predicted to be slightly stronger in the Dd Mg structure than in the Ch_{giz} structure (Figs. 5 and 7). In Dd Mg, Glu-187 also forms a H-bond from O_ϵ to a nearby water. This interaction is also seen in the x-ray crystal structure. In both Dd Mg and Ch_{giz} we predict a contact between Thr-186 H_γ and Asp-454 O_δ (1.07 and 1.62 Å, respectively) that is not observed in either crystal structure. The most disparate measures are from the backbone NH of Gly-184 to O_β of ATP, with both MM and CP predicting an almost 0.4 Å greater hydrogen bond in the Ch_{giz} structure.

When we turn to the Dd Ca simulations (Fig. 6), the unequal interaction of Lys-185 with the nucleotide phosphates is less pronounced. The H_ζ–O_γ distance is 1.61 Å and the H'_ζ–O_β distance is 1.55 Å, making the differences in these quantities the same as in our Ch_{giz} simulations, i.e., Lys-185 appears to (slightly) stabilize the β-phosphate more than the γ-phosphate. This is reasonable given the transition state conformation of the protein. One additional factor might be an extra hydrogen bond formed between H_ϵ of Lys-185 and an O_δ of Asp-454 (not shown in Fig. 6), thus pulling the side chain of Lys-185 back just enough to distort any conformation that might hint at the general acid character alluded to, as in the case of Dd Mg.

Regardless, we can say that Lys-185 interacts most markedly with the nucleotide when the nucleotide and the protein are both in prehydrolysis conformations as observed in Dd Mg (Fig. 5). The P-loop in Dd Ca (Fig. 6) does not preserve the hydrogen bond from the backbone NH of Gly-184 to O_β, but instead establishes a new bond to the bridging, $O_{\beta\alpha}$, oxygen in ATP. This is presumably because CaATP is in a different position in the P_i-tube than is MgATP, the template for the CaATP simulations. Similarly, the Thr-186 H_γ and Asp-454 O_δ interaction is missing in the Dd Ca structure and has been replaced instead by a Thr-186 H_γ–O_α H-bond. The contact to Ca^{2+} from the O_γ of Thr-186 is weaker than observed in the Dd Mg or Ch_{giz} cases (almost 2.4 Å vs. ~2 Å), as is that of the backbone amide hydrogen of Glu-187 to the O_α of the nucleotide.

Switch 1 and switch 2

As in the P-loop, there are a number of potentially reactive components of switch 1 and switch 2. In switch 1, the universally conserved moieties include three residues with polar side chains (Asn-233, Ser-236, and Ser-237) and one

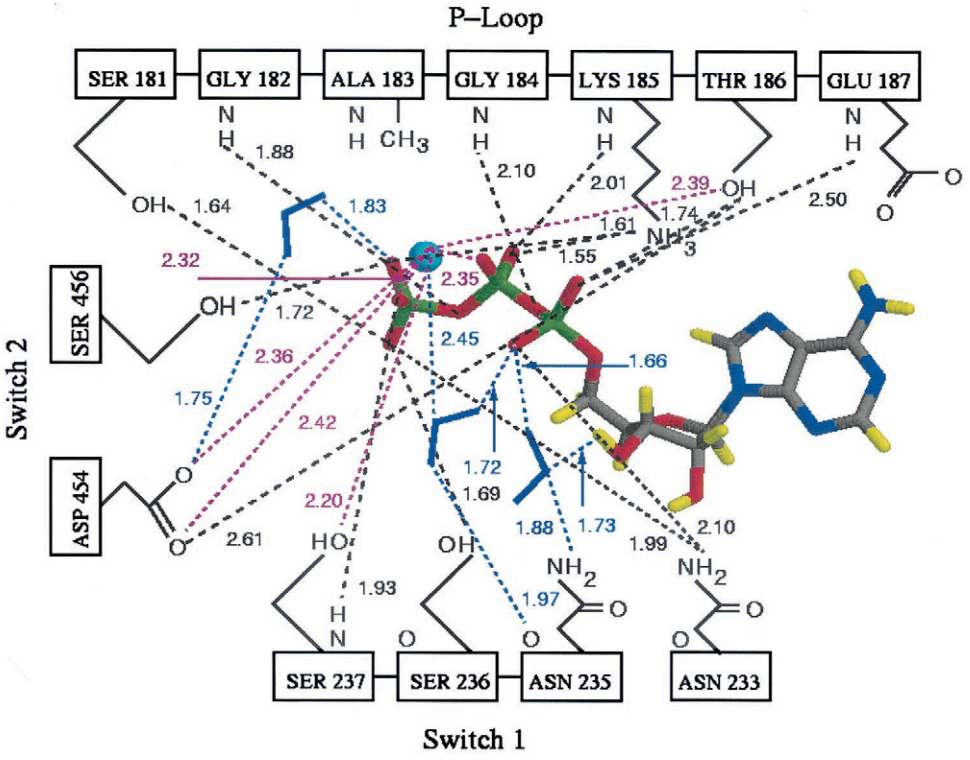

FIGURE 6 The hydrogen-bonding pattern in the active site when CaATP was considered as the nucleotide in the Dd S1 structure. Ca^{2+} is the light blue sphere and is coordinated sevenfold. The color scheme for the nucleotide is as in Fig. 5. H-bonds involving water are colored blue and, for clarity, six of the seven interactions to the metal are colored magenta. Of the seven, one is a metal-water interaction and the other is a hard-to-discern metal to γ-phosphate oxygen ionic interaction. Because there is no crystal structure of Dd S1 complexed with a CaATP analog, we cannot compare our results with experiment; however, we do note that this structure represents the first published report of myosin complexed with CaATP.

residue that carries a formal charge of +1, Arg-238. However, it is evident from crystal structures that Arg-238 does not interact with either an ATP analog (Fisher et al., 1995) or a transition state analog (Smith and Rayment, 1996a). In switch 2 there are three universally conserved residues, two of which (Asp-454 and Glu-459) carry formal charges of −1. In the x-ray crystal structure of Dd complexed with an MgATP analog, there is a single interaction between what would be the γ-phosphate of ATP and switch 2, and the interaction is a weak one. Asp-454 is H-bonded to a water, which is in turn H-bonded to one of the γ-phosphate oxygens. In the x-ray crystal structure of Ch_{giz}, switch 2 is displaced almost 4 Å closer to the γ-phosphate mimic of the nucleotide analog. As a result, switch 2 interacts directly with the substrate via a hydrogen bond formed from the backbone amide hydrogen of Gly-457 to one of the γ-phosphate oxygens.

The greatest number of direct contacts—and by direct, we include the bound metal cation— between switch 1 and the nucleotide involve Ser-237. The O_γ of Ser-237 interacts with the metal in all three cases studied (confirmed in crystal structures for Dd Mg and Ch_{giz}). The backbone oxygen of Ser-237 is involved in stabilizing a nearby water only in the Dd Mg structure. In the two other cases we consider, there is no water present in the required location for this interaction to form. In Dd Mg the H_γ of Ser-237 forms a hydrogen bond with a nearby water. In Ch_{giz}, H_γ is coordinated with Asp-454. In Dd Ca, MM simulations show that H_γ forms an intramolecular hydrogen bond with the backbone oxygen of Ser-237, presumably because putative electron donors are either absent (as in the case of the water) or displaced from Ser-237 by such a distance that precludes a meaningful interaction (as in the case of Asp-454). We note that none of these interactions is observed in the available crystal structures because hydrogens are not resolved in those experiments.

In all three systems, H_γ of Ser-236 hydrogen bonds to an O_γ of ATP. This H-bond is alluded to in the crystal structures of Dd Mg and Ch_{giz}, but as in the case of H_γ of Ser-237, was not confirmed until our simulations were completed. In the Dd prehydrolysis x-ray structure, Ser-236 is hypothesized to hydrogen-bond to both the γ-phosphate and one of the charged amino groups of the side chain of Arg-238. This latter interaction is observed in the MM simulations but not in the CP refinements, due to the exclusion of Arg-238 in the model. In the crystal structure with a transition state nucleotide bound at the active site, Ser-236 is shown to take on a more important role, namely

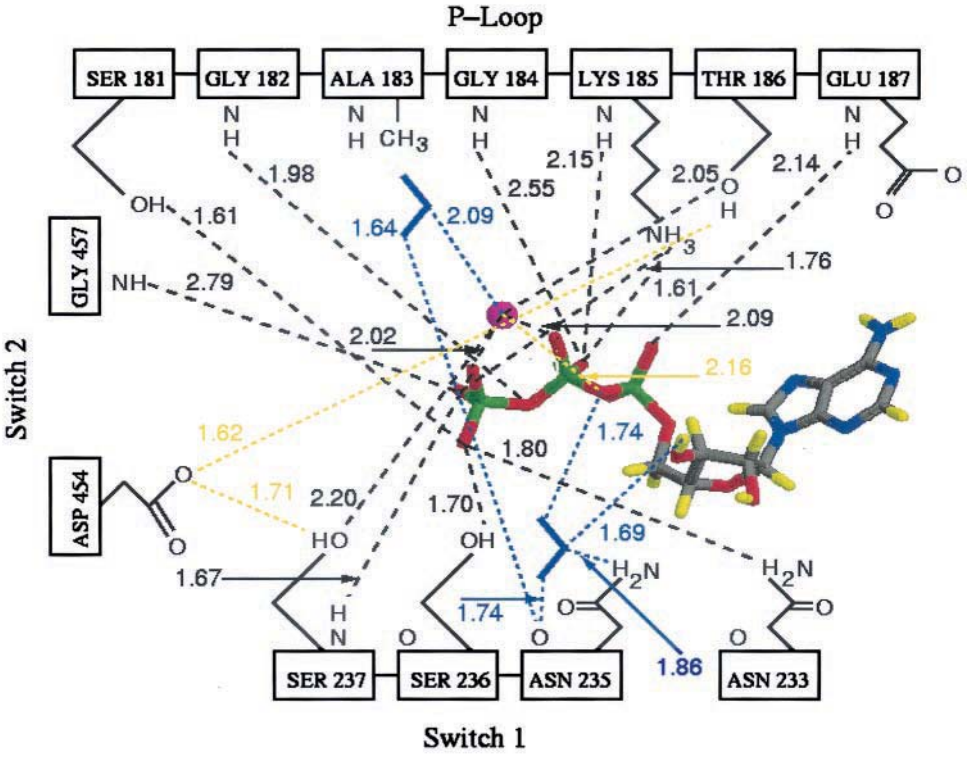

FIGURE 7 The hydrogen-bonding pattern in the active site of the Ch_{giz} S1 structure with MgATP as the nucleotide. The reader is reminded that the numbering of the aa residues in this figure is that for the Dd structure. The proper numbering in the Ch_{giz} S1 structure is as follows: switch 1, aa 242-247; switch 2, aa 465-470; P-loop, aa 177-184; and the switch 2 α-helix, aa 478-508. The universally conserved Asp and Gly residues in switch 2 are numbered 465 and 468, respectively, in the x-ray crystal structure. Both waters were not removed before the simulations—this is explained in Methods—and remain where the x-ray structure pinpoints them. As in Figs. 5 and 6, the color scheme for the nucleotide atoms is the same, including the magnesium. Interactions between Thr-186 H_γ and Asp-454 O_δ, Asp O_δ and Ser-237 H_γ, and Mg^{2+} and one of the α-phosphate oxygens of the nucleotide were not observed in the crystal structure and are accordingly indicated with yellow lines. Finally, water interactions are in blue.

that of stabilizing the equatorial oxygens of the trigonal bipyramidal P_i leaving group. We fail to observe any of these interactions in our simulations, most likely because the nucleotide is not in its transition state.

We next consider Asn-235. The function of this residue appears to be that of stabilizing either one or two water molecules. If the Dd x-ray crystal structures are used as a guide, then Asn-235 forms two H-bonds, one per each of two waters (neither of them lytic), if the prehydrolysis nucleotide is bound. At the transition state, the crystal structure shows the two H-bonds from Asn-235 terminating at one water molecule. Our simulations of Dd Mg (Fig. 5) indicate that Asn-235 only interacts with one water, forming a single H-bond of ~1.8 Å that emanates from the backbone oxygen of the amino acid. We see the "two H-bonds with two waters"-type structures when CaATP is the nucleotide (Fig. 6) or if Ch_{giz} (Fig. 7) is considered. In the two Dd x-ray structures, the water that is always in contact with Asn-235 is also always in contact with Mg^{2+}. Similarly, that is the case for the CaATP and Ch_{giz} simulations. Only in our simulation of Dd Mg do we not observe any interaction of Asn-235 to a water that is also bound to the metal.

The last of the four residues from switch 1 that is included in the CP structural refinements is Asn-233. This residue is known to form an H-bond from the side chain amino group to one of the γ-phosphate oxygens (this is observed in the x-ray structure and in our simulations). In the Ch_{giz} structure this contact is preserved, as it is in the x-ray structure of Dd complexed with a transition state nucleotide analog. If CaATP is the nucleotide, we predict that additional stabilization of the nucleotide occurs through an H-bond formed to one of the α-oxygens of ATP (Fig. 6). This feature is seen in the x-ray structure of Dd Mg but not in that of Ch_{giz}, or when Dd binds a transition state nucleotide in the active site.

In switch 2 we include Asp-454 in all the simulations. The water-mediated H-bond to a γ-oxygen of ATP in the crystal structure of Dd Mg is reproduced (Fig. 5) and is predicted to be present if CaATP is the nucleotide (Fig. 6). For all models studied, Asp-454 forms an H-bond with Thr-186, a feature not observed in any Dd x-ray crystal structure. MM simulations suggest, and CP refinements confirm, that when Ca^{2+} is substituted for Mg^{2+}, additional coordination of the metal and nucleotide to switch 2 results:

Asp-454 has two additional H-bonds (both to Ca^{2+}) and Ser-456 is close enough to form a 1.7 Å bond with one of the γ-oxygens of CaATP. In the Ch_{giz} crystal structure, the backbone amide N of Gly-457 is 3.12 Å from one of the γ-phosphate oxygens. In the course of our MM simulations, the distance narrowed to 2.87 Å and subsequent CP refinements of the structure (Fig. 7) give a value of 2.79 Å (note that this is the only distance on Figs. 5–7 that does not have the heavy atom to hydrogen distance subtracted from it). When the N–H bond distance is subtracted from this quantity, a hydrogen bond on the order of 1.8 Å is realized. This is more than sufficient to promote hydrolysis.

Coordination of waters and the metal

We preface this section with a comment about the MM simulation of the Dd Mg structure. The initial positioning of the waters was random and there were any number of structures that could have resulted as the simulations evolved in time. The fact that the key waters at the nucleotide site that were resolved crystallographically "found their way home" and were also resolved computationally gives greater confidence in our simulations and further validates the results. Of particular interest was the water that has previously been suggested to be involved in the hydrolysis of the γ-phosphate of MgATP via an in-line S_N2 attack (Kagawa and Mori, 1999). In Fig. 5 this water is the one located in the lower left-hand corner of the figure. The position of this water was especially well-reproduced when compared to crystallographic data (Fisher et al., 1995).

All three crystal structures examined (Dd S1 · MgADP · BeF_x; Dd S1 · MgADP · VO_4, PDB 1VOM; and Ch_{giz} S1 · MgADP · BeF_x) do not indicate bonding between Mg^{2+} and one of the α-phosphate oxygens. In both MM and CP simulations, Mg^{2+} is coordinated to ATP via one of the α-phosphate oxygens; coordination to the β- and γ-phosphate oxygens is reproduced. The CP simulations yield values that agree with the x-ray structure most closely and indicate that the metal is too tightly bound to the triphosphate in the MM simulations. In the Dd Mg and Ch_{giz} simulations, Mg^{2+} fills out its coordination with ionic interactions with a nearby water, Thr-186, and Ser-237. When Ca^{2+} is considered, the metal–α-phosphate linkage is lost and two new hydrogen bonds, both to Asp-454, are formed, yielding a sevenfold coordinate Ca^{2+} (the contacts to a water, the β- and γ-phosphates, Thr-186, and Ser-237 are preserved as in Dd Mg and Ch_{giz}).

There exist markedly different water coordinations in the Dd Mg and Ch_{giz} crystal structures. Only two waters are crystallographically resolved for Ch_{giz}, while at least six waters are shown to be in the P_i-tube in Dd Mg. In MM and CP simulations of Dd Mg (Fig. 5), a water is hydrogen-bonded to a P_γ oxygen, O_γ of Ser-237, and another water, which is itself coordinated with Mg^{2+}. The third water is stabilized by Glu-187 and the H_γ of Ser-237, while the fourth water simply forms a hydrogen bond with Asp-454. For the Ch_{giz}-structure (Fig. 7), the water closest to the Mg^{2+} coordinates with it and the O_γ of Ser-237, seemingly mimicking the second water in the Dd Mg structure. The second water present forms a hydrogen bond with the 3′-hydroxyl on the ribose of ATP and again, the simulations accurately predict this structure.

When we consider Dd Ca (Fig. 6), the water most likely to be the lytic water forms a hydrogen bond with Asp-454 (1.76 Å) and one with the same γ-phosphate oxygen that is hydrogen-bonded to Ser-456 (1.84 Å). As in the Ch_{giz} simulation, there is a water interacting with the 3′-hydroxyl on the ribose of ATP. This water hydrogen-bonds with one of the α-phosphate oxygens as well.

Bond lengths and angles within ATP

One of the yardsticks we can use to gauge the efficacy of our methods is to examine the bond lengths and angles in the nucleotide. In an MM force field, electrons are considered to be localized on atoms, giving rise to partial charges. This assumption is generally a valid one, and we note that the RESP procedure (Bayly et al., 1993) that is used when deriving charges for atoms in molecules that are are not included as part of standard AMBER force field (such as ATP) has the effect of "smearing" the atom-centered charges to better approximate a more realistic picture of electron delocalization. However, even though the RESP procedure is a step in the right direction, the resulting charges are fixed and cannot be adjusted, if and when the local environment is dynamic enough to warrant continuous updating of the electronic structure of the system. In the present study we are faced with a highly charged, relatively small nucleotide (44 atoms for ATP plus a cation) in which the electrons are certainly delocalized over much of the triphosphate arm. Because there are many reactive amino acids present in the active site, the electrons become more delocalized still. Using a QM technique allows us to more accurately establish the geometry of the system as long as the level of theory at which we do the calculation is itself sufficiently robust.

The calculated β-oxygen to P_β distances (both MM and CP) are indistinguishable from the values reported for the x-ray crystal structures of Dd Mg and Ch_{giz}. In these crystal structures, the γ-position P–O bonds are very slightly longer than the β-position P–O distances. CP reproduces this trend, but not MM, which sets these five bond lengths to equal one another. The $O_{\gamma\beta}$–P_γ bond should be longer than the $O_{\gamma\beta}$–P_β bond. Both MM and CP simulations reproduce this trend. However, the CP distances are closer to the values obtained by crystallography. Similarly, the trend is followed when the β- to α-linkage is considered.

One commonly accepted theme when discussing the structure of ATP bound to the protein is that the γ-phosphate oxygen atoms are in a tetrahedral arrangement. In the

crystal structure, the γ-phosphate group is mimicked by a nonhydrolyzable BeF_3 group bound to MgADP. The three angles formed by the F atoms, the Be atom, and the oxygen on ADP that was to mimic $O_{\gamma\beta}$, are 108.4°, 108.4°, and 109.6°. The average is thus 108.8°, meaning that the BeF_x group geometry deviates from that of a perfect tetrahedron by only 0.7°. In reality, however, we expect more deviation because of the many varied forces interacting with the triphosphate arm in general, and the γ-phosphate in particular.

The three O_γ–P_γ–$O_{\gamma\beta}$ angles are calculated to be significantly less than the almost perfectly tetrahedral quantities observed in the crystal structures. Both CP and MM values (103.5° and 103.8°, respectively) indicate that the terminal phosphate is strained by almost 6°. The P_γ–$O_{\gamma\beta}$–P_β angle—observed to be ~135° in both the Dd Mg and Ch_{giz} structures—is more closely approximated by CP (126° and 122°) than MM (120° and 118°). The same trend is observed for the P_β–$O_{\beta\alpha}$–P_α angle.

DISCUSSION

We have used classical molecular mechanical and quantum mechanical methods to examine the stability of the crystal structures of Ch_{giz} and Dd S1 myosin, the interaction of the nucleotide with the motor protein, and the implications of variation in the cation associated with the nucleotide. Crystal structures are static pictures of conformations of proteins, and thus finer details of complex portions of the systems, such as where intricate hydrogen bonding patterns are crucial, may not be accurately reported for an aqueous environment at physiological temperatures. The modeling approaches used here give us extremely powerful tools to predict structural, mechanistic, and energetic properties of biomolecules that can supplement the knowledge gained from x-ray crystallography.

Our modeling indicated that all three structures considered were stable nucleotide-motor conformations under physiological conditions. This suggested that they represented viable conformations during the ATP hydrolysis cycle. Free energy calculations showed that the Dd Mg structure binds MgATP more tightly than Ch_{giz}. Our calculated ΔG_{bind} for Dd S1 · MgATP was −16 kcal/mol, in excellent agreement with experimental quantities. Within the limits of our simulation tools, we have also provided refined estimates under more physiological conditions of hydrogen bonds that have been identified in the crystal structures, and have suggested new contacts that have not previously been suggested.

The Ch_{giz} x-ray structure has a closed switch 2 conformation. The closing of switch 2 was originally seen in Dd structures with either MgADP · AlF_4^- or MgADP · VO_4 at the nucleotide site. This led to the hypothesis that switch 2 movements were involved in both stabilizing the nucleotide transition state intermediate during hydrolysis and, via movements transmitted through the switch 2 α-helix, in driving the powerstroke. The ATP analog state with a closed switch 2 has brought into question the exact structural relationship between hydrolysis and motion.

Several modeling observations now allow us to place the open and closed switch 2 structures in better perspective. Surprisingly, the simulations indicate that at the γ-phosphate position, the nucleotide in the Dd MgATP structure (open switch 2) has partly undergone a transition to the nucleotide hydrolysis transition state intermediate. The bond angles between the γ-phosphate oxygens, the γ-phosphorus, and the P_γ–P_β bridging oxygen average ~103° in the simulations. This is a 6° deviation from the 109.5° angle expected for a true ATP at the active site. This latter angle is the one in the Dd MgADP · BeF_x crystal structure. In perspective, the 6° deviation from ideality is 30% of the magnitude change needed for a distortion to the 90° angle of the true hydrolysis transition intermediate. A similar angular change at the γ-phosphate position toward the transition state nucleotide is also seen in the Ch_{giz} MgATP simulations.

In the closed switch 2 conformation of the Dd MgADP · AlF_4^- and the Dd MgADP · VO_4 crystal structures, there is a salt bridge between Glu-459 in switch 2 and Arg-238 in switch 1 (Glu-459 O_ϵ to Arg-238 H distances are 1.73 and 1.80 Å). This salt bridge is not observed in the Dd MgADP · BeF_x structure, leading to suggestions that the formation of this salt bridge is a part of the closing of switch 2 (reviewed in Geeves and Holmes, 1999). The interactions we observe in the Ch_{giz} MgATP structure are significantly weaker (1.92 and 2.11 Å distances) than in the Dd closed switch 2 structures. The weaker salt bridge, along with the modification of the positions of the γ-phosphate oxygens to a strained-tetrahedral configuration, suggest that the closed switch 2 state with MgATP at the active site may actually be an intermediate on the path to the true transition state, as exemplified by the Dd structures with MgADP · AlF_4^- or MgADP · VO_4 at the nucleotide site.

The role of Lys-185

Our simulations indicate that the universally conserved Lys-185 residue in the P-loop interacts with the nucleotide in a way such that this residue may play the role of a general acid in the hydrolysis reaction. This conclusion differs from that of Kagawa and Mori (1999), who used a semi-empirical method to analyze the molecular orbitals of MgATP in the active site of the Dd MgADP · BeF_x structure. Quantum mechanical calculations done at the semi-empirical level of theory are implicitly parametrized, and therefore some bias in the results of these calculations can be expected. They modeled Lys-185 as neutrally charged (i.e., possessing two instead of three hydrogens at the N_ζ position). Lys-185 was thus suggested to act as a general base that extracts a proton from the lytic water and then forms the attacking hydroxyl

group. The pK_a of an acidic ζ proton is ~10.5 and there are waters present nearby, which would appear to make deprotonation difficult. It has been shown, however, that the pK_a of the acidic proton of lysine can be lowered by as many as 4.5 $\log_{10}$ units (Paetzel et al., 1997). This phenomenon occurs in the binding site of the *Escherichia coli* signal peptidase (Paetzel et al., 1997, 1998), and results in a nearby serine losing the Hγ from its side chain, thus transforming the serine into a nucleophile that cleaves a bound substrate. However, Paetzel and co-workers concluded that for lysine to function as a general base, it must be located in either a hydrophobic domain or there must be a local net positive charge. Clearly, neither of these conditions is true in the active site of myosin. There is instead water present and the net charge of the metal-ATP complex is strongly negative. We suggest that Lys-185 is protonated and acts a general acid if it is involved in a capacity beyond that of stabilizing the triphosphate arm of ATP during hydrolysis.

Lys-185 can act as a general acid and function to stabilize a structural state depending upon which conformer of the protein is examined, given the same nucleotide at the active site. When MgATP is placed in the Dd S1 structure (i.e., the prehydrolysis conformation of S1), Lys-185 forms a stronger hydrogen bond with one of the γ-phosphate oxygens than it does with a β-phosphate oxygen. The converse is observed when MgATP is bound to the Ch_{giz} transition state structure, and is consistent with the hypothesis that Lys-185 is an important contributor to the hydrolysis cycle. In fact, it is the only amino acid positioned in the proper manner to do duties as an electron acceptor in the prehydrolysis step and then stabilize MgADP after the P_γ–$O_{\gamma\beta}$ bond has been broken. When CaATP is positioned into the nucleotide-binding site, Lys-185 is too far away from the phosphate arm to significantly act in a biased way toward either of the γ- or β-phosphates, and therefore cannot play as important a role in hydrolysis as it does in Dd Mg. As discussed in the next subsection, this is not an apparent contradiction. Although the net ATP turnover rate increases when CaATP is the substrate, the modeling suggests that this is not due to a faster hydrolysis step, but rather to faster dissociation of the product P_i. This agrees with the observation that the rate-determining step for the hydrolysis cycle of MgATP is the dissociation of P_i from the metal-ADP complex (Taylor, 1979).

Active-site metal and water coordination

Recalling that switch 2 is in the open configuration in the Dd Mg structure and closed in the Ch_{giz} structure, it is not unreasonable that fewer crystallographic waters are resolved in the latter case than in the former. There simply is not enough room in the P_i-tube to accommodate them. In the Dd simulations, it is clear that a lytic water hydrogen-bonds to the γ-phosphate oxygen and participates in the in-line S_N2 attack of the γ-phosphorus. The situation is not so obvious in the Ch_{giz} crystal structure and in our simulations.

In the Ch_{giz} x-ray structure and in the results of our simulations (Fig. 7), one of the two waters present in the P_i-tube is retained by two H-bonds to Asn-235 and two H-bonds to the nucleotide. The other water interacts with Asn-235 (via one H-bond) and the Mg^{2+} cation (also one H-bond). In the Dd Mg crystal structure (Fisher et al., 1995), it is obvious that the lytic water is the one that does not have any interactions at all with the Mg^{2+} cation. This is confirmed in the crystal structure of Dd complexed with a transition state analog of the nucleotide (Smith and Rayment, 1996a), because the only other candidate in the proper position remains bound to the metal cation (this distance is reported as 2.1 Å for both crystal structures). We can therefore conclude that one of the requirements of the lytic water is that it not be bound to the highly charged cation.

In the Ch_{giz} x-ray structure the distance from the oxygen of the metal-bound water to the metal is 2.15 Å (our simulations yield 2.09 Å; either number is quite close to the distance reported for the Dd structures). It is not this water that attacks the γ-phosphate of ATP. The other water is tightly bound via four H-bonds to portions of the P-loop and the nucleotide, which precludes it from being the lytic water. The most reasonable explanation for the absence of the lytic water is the one that was given above; that is, that there just is not enough room in the P_i-tube. An alternative explanation is that if the Ch_{giz} structure represents the enzyme in its transition state, then we can hardly expect the water that is consumed in the hydrolysis reaction to be present. Is it possible that the x-ray crystal structure of Ch_{giz} has captured the enzyme in the transition state while binding a prehydrolysis analog of MgATP?

In Dd Ca the lytic water is present and mediates a hydrogen bond between Ser-456 and the γ-phosphate of ATP. The metal is coordinated sevenfold as opposed to the sixfold coordination seen in the Dd Mg simulations, and has greater communication with switch 2 as a result. The rate-limiting step in the myosin MgATPase is the release of phosphate from the myosin · MgADP · P_i state (reviewed in Taylor, 1979); the rate-limiting step in the myosin CaATPase has not been established. However, the nature of the coordination of Ca^{2+} would result in the faster release of P_i from the ADP · P_i state when Ca^{2+} is the metal instead of Mg^{2+}. There are simply stronger bonds among Mg^{2+}, the nucleotide, and nearby protein residues that retain the leaving group more so than Ca^{2+} does. We can thus hypothesize that an enhanced P_i release rate is responsible for the enhanced myosin CaATPase rate.

The MM and CP calculations provide qualitatively similar results concerning trends in bond lengths and angles. However, as noted earlier, one of the major differences lies in the treatment of the metal cation. MM shows much tighter binding of the metal to surrounding ligands and/or water, while CP yields distances much closer to experiment.

This factor is extremely important because if the metal is too acidic (i.e., too tightly bound to the triphosphate), we will not see P_i release in the requisite time (T. J. Minehardt, N. Marzari, R. Cooke, E. Pate, and R. Car, unpublished observations).

Validation of the pseudopotential and exchange-correlation functional

Finally, we have shown that Vanderbilt ultrasoft pseudopotentials and the PBE exchange-correlation functional used in this study are appropriate for biological systems. Thus far, the Car-Parrinello formalism has been implemented for biological systems—that is, systems where the chemistry of the solvent and weakly bonded interactions must be accurately portrayed—by using Troulliers-Martins pseudopotentials (Becke, 1988), the exchange functional of Becke (1988), and the correlation functional of Lee et al. (1988).

The computational cost and limit on the size of the system that can be investigated by CP molecular dynamics depends critically on the "softness" of the pseudopotential. A smoother pseudopotential allows one to reduce the number of elements in the plane-wave basis set that are necessary to approximate completeness. A high-energy cutoff for the basis set—and thus a high computational cost—is a requirement if one uses traditional norm-conserving pseudopotentials, such as the Troulliers-Martins type. By using Vanderbilt ultrasoft pseudopotentials (Vanderbilt, 1990), a low-energy cutoff (c.f. 25 Ry to ~70 Ry for the studies mentioned above) can be used, allowing us to investigate a very large system (by quantum mechanical standards) at an affordable computational cost. For the systems studied this translates into a reduction from roughly 590,000 plane waves in the basis set for the norm-conserving case to 126,000 in the ultrasoft case. Time-reversal symmetry allows for a further reduction of a factor of 2 in the size of the basis set.

The combination of the Becke and Lee et al. functionals—known collectively as the BLYP exchange-correlation functional—enjoys widespread use (Alber et al., 1999a, b; Alber and Carloni, 2000; Pantano et al., 2000; Piana and Carloni, 2000; Rothlisberger et al., 2000; Sulpizi and Carloni, 2000; Cecconi et al., 2001; Dal Peraro et al., 2001) because, among other things, it accurately reproduces hydrogen-bonding patterns that are observed experimentally (Parrinello, 1997; Tuckerman et al., 1995; Molteni and Parrinello, 1998). We have shown that the PBE exchange-correlation functional (Perdew et al., 1996, 1997) is capable of refining the structure of a highly H-bonded system while suggesting electronic interactions not accurately calculated by MM simulations. In the present study we considered only the interaction of the nucleotide with myosin, not the hydrolysis *reaction* itself. However, our results suggest the applicability of the Vanderbilt-PBE combination to analyses of the full hydrolysis reaction at the active site of myosin. These calculations are in progress.

T.J.M. is a Princeton University Council on Science and Technology (CST) Postdoctoral Fellow. This work was also supported by U.S. Public Health Service Grants AR39643 (to E.P.), AR42895 (to R. Cooke), and GM29072 (to P.A.K.). We gratefully acknowledge the Princeton University W. M. Keck Foundation Materials Science Computing Center for access to and the use of their computing resources.

REFERENCES

Alber, F., and P. Carloni. 2000. Ab initio molecular dynamics studies on HIV-1 reverse transcriptase triphosphate binding site: implications for nucleoside-analog drug resistance. *Protein Sci.* 9:2535–2546.

Alber, F., G. Folkers, and P. Carloni. 1999a. Dimethyl phosphate: stereoelectric versus environmental effects. *J. Phys. Chem. B.* 103:6121–6126.

Alber, F., G. Folkers, and P. Carloni. 1999b. Conformational analysis of dimethyl phosphate in aqueous solution: a density functional theory-based molecular dynamics study. *J. Mol. Struct. (Theochem.).* 489: 237–245.

Aqvist, J. 1992. Modelling of ion-ligand interactions in solutions and biomolecules. *J. Mol. Struct. (Theochem.).* 256:135–152.

Bashford, D., D. A. Case, C. Choi, and G. P. Gippert. 1997. Computational study of the role of solvation effects in reverse turn formation in the tetrapeptides APGD and APGN. *J. Am. Chem. Soc.* 119:4964–4971.

Bayly, C. I., P. Cieplak, W. D. Cornell, and P. A. Kollman. 1993. A well-behaved electrostatic potential based method using charge restraints for deriving atomic charges: the RESP model. *J. Phys. Chem.* 97:10269–10280.

Becke, A. D. 1988. Density functional exchange-energy approximation with correct asymptotic behaviour. *Phys. Rev. A.* 38:3098–3100.

Berendsen, H. J. C., J. P. M. Postma, W. F. van Gunsteren, A. DiNola, and J. R. Haak. 1984. Molecular dynamics with coupling to an external bath. *J. Chem. Phys.* 81:3684–3690.

Car, R., and M. Parrinello. 1985. Unified approach for molecular-dynamics and density-functional theory. *Phys. Rev. Lett.* 55:2471–2474.

Case, D. A., D. A. Pearlman, J. W. Caldwell, T. E. Cheatham III, W. S. Ross, C. L. Simmerling, T. A. Darden, K. M. Merz, R. V. Stanton, A. L. Cheng, J. J. Vincent, M. Crowley, V. Tsui, R. J. Radmer, Y. Duan, J. Pitera, I. Massova, G. L. Seibel, U. C. Singh, P. K. Weiner, and P. A. Kollman. 1999. AMBER 6. University of California, San Francisco.

Cecconi, F., C. Micheletti, P. Carloni, and A. Maritan. 2001. Molecular dynamics studies on HIV-1 protease drug resistance and folding pathways. *Proteins.* 43:365–372.

Chong, L. T., Y. Duan, L. Wang, I. Massova, and P. A. Kollman. 1999. Molecular dynamics and free-energy calculations applied to affinity maturation in antibody 48G7. *Proc. Natl. Acad. Sci. U.S.A.* 96: 14330–14335.

Cooke, R. 1997. Actomyosin interaction in striated muscle. *Physiol. Rev.* 77:671–691.

Cornell, W. D., P. Cieplak, C. I. Bayly, I. R. Gould, K. M. Merz, D. M. Ferguson, D. C. Spellmeyer, T. Fox, J. W. Caldwell, and P. A. Kollman. 1995. A second generation force field for the simulation of proteins, nucleic acids, and organic molecules. *J. Am. Chem. Soc.* 117: 5179–5197.

Dal Peraro, M., F. Alber, and P. Carloni. 2001. Ser133 phosphate-KIX interactions in the CREB-CBP complex: an ab initio molecular dynamics study. *Eur. Biophys. J.* 30:75–81.

Demchuk, E., D. Bashford, G. Gippert, and D. A. Case. 1997. Thermodynamics of a reverse turn motif. Solvent effects and side-chain packing. *J. Mol. Biol.* 270:305–317.

Dominguez, R., Y. Freyzon, K. M. Trybus, and C. Cohen. 1998. Crystal structure of a vertebrate smooth muscle myosin motor domain and its complex with the essential light chain: visualization of the pre-power stroke state. *Cell.* 94:559–571.

Fisher, A. J., C. A. Smith, J. B. Thoden, R. Smith, K. Sutoh, H. M. Holden, and I. Rayment. 1995. X-ray structures of the myosin motor domain of *Dictyostelium discoideum* complexed with MgADP · BeF_x and MgADP · AlF_4^-. *Biochemistry.* 34:8960–8972.

Geeves, M. A., and K. C. Holmes. 1999. Structural mechanism of muscle contraction. *Annu. Rev. Biochem.* 68:687–728.

Gulick, A. M., C. B. Bauer, J. B. Thoden, E. Pate, R. G. Yount, and I. Rayment. 2000. X-ray structures of the *Dictyostelium* myosin motor domain with six non-nucleotide analogs. *J. Biol. Chem.* 275:398–408.

Gulick, A. M., C. B. Bauer, J. B. Thoden, and I. Rayment. 1997. X-ray structures of the MgADP, $MgATP_\gamma S$, and MgAMPPNP complexes of the *Dictyostelium discoideum* myosin motor domain. *Biochemistry.* 36: 11619–11628.

Gulick, A. M., H. Song, S. A. Endow, and I. Rayment. 1998. X-ray crystal structure of the yeast Kar3 motor domain complexed with Mg-ADP to 2.3 Angstrom resolution. *Biochemistry.* 37:1769–1776.

Holmes, K. C. 1996. Muscle proteins: their actions and interactions. *Curr. Opin. Struct. Biol.* 6:781–789.

Honig, B., K. Sharp, and A. S. Yang. 1993. Macroscopic models of aqueous solutions: biological and chemical applications. *J. Phys. Chem.* 97:1101–1109.

Houdusse, A., V. N. Kalabokis, D. Himmel, A. G. Szent-Gyorgyi, and C. Cohen. 1999. Atomic structure of scallop myosin subfragment S1 complexed with MgADP: a novel conformation of the myosin head. *Cell.* 97:459–470.

Jorgensen, W. L., J. Chandrasekhar, J. D. Madura, R. W. Impey, and M. L. Klein. 1983. Comparison of simple potential functions for simulating liquid water. *J. Comput. Phys.* 79:926–935.

Kagawa, H., and K. Mori. 1999. Molecular orbital study of the interaction between MgATP and the myosin motor domain: the highest occupied molecular orbitals indicate the reaction site of ATP hydrolysis. *J. Phys. Chem. B.* 103:7346–7352.

Kozielski, F., S. Sack, A. Marx, M. Thormahlen, E. Schonbrunn, V. Biou, A. Thompson, E. M. Mandelkow, and E. Mandelkow. 1997. The crystal structure of dimeric kinesin and implications for microtubule-dependent motility. *Cell.* 91:985–994.

Kull, F. J., E. P. Sablin, R. Lau, R. J. Fletterick, and R. D. Vale. 1996. Crystal structure of the kinesin motor domain reveals a structural similarity to myosin. *Nature.* 380:550–555.

Kull, F. J., R. D. Vale, and R. J. Fletterick. 1998. The case for a common ancestor: kinesin and myosin motor proteins and G proteins. *J. Muscle Res. Cell Motil.* 19:877–886.

Lee, C., W. Yang, and R. C. Parr. 1988. Development of the Cole-Salvetti correlation energy formula into a functional of the electron density. *Phys. Rev. A.* 37:785–789.

Massova, I., and P. A. Kollman. 1999. Computational alanine scanning to probe protein-protein interactions: a novel approach to evaluate binding free energies. *J. Am. Chem. Soc.* 121:8133–8143.

Minehardt, T. J., R. Cooke, E. Pate, and P. A. Kollman. 2001. A molecular dynamics study of the energetic, mechanistic, and structural implications of a closed phosphate tube in ncd. *Biophys. J.* 80:1151–1168.

Molteni, C., and M. Parrinello. 1998. Glucose in aqueous solution by first principles molecular dynamics. *J. Am. Chem. Soc.* 120:2168–2171.

Müller, J., A. Marx, S. Sack, Y. H. Song, and E. Mandelkow. 1999. The structure of the nucleotide-binding site of kinesin. *Biol. Chem.* 380: 981–992.

Osapay, K., W. Young, D. Bashford, C. L. Brooks III, and D. A. Case. 1996. Dielectric continuum models for hydration effects on peptide conformational transitions. *J. Phys. Chem.* 100:2698–2705.

Paetzel, M., R. E. Dalbey, and N. C. J. Strynadka. 1998. Crystal structure of a bacterial signal peptidase in complex with a β-lactam inhibitor. *Nature.* 396:186–190.

Paetzel, M., N. C. J. Strynadka, W. R. Tschantz, R. Casareno, P. R. Bullinger, and R. E. Dalbey. 1997. Use of site-directed chemical modification to study an essential lysine in *Escherichia coli* leader peptidase. *J. Biol. Chem.* 272:9994–10003.

Pantano, S., F. Alber, and P. Carloni. 2000. Proton dynamics in an enzyme model substrate: an ab initio molecular dynamics study. *J. Mol. Struct. (Theochem.).* 530:177–181.

Parr, R. G., and W. Yang. 1989. Density-functional theory of atoms and molecules. Oxford University Press, New York.

Parrinello, M. 1997. From silicon to RNA: the coming age of ab initio molecular dynamics. *Solid State Comm.* 102:107–120.

Pate, E., K. L. Nakamaye, K. Franks-Skiba, R. G. Yount, and R. Cooke. 1991. Mechanics of glycerinated muscle fibers using nonnucleoside triphosphate substrates. *Biophys. J.* 59:598–605.

Pearlman, D. A., D. A. Case, J. W. Caldwell, W. S. Ross, T. E. Cheatham III, S. DeBolt, D. Ferguson, G. Seibel, and P. A. Kollman. 1995. AMBER, a package of computer programs for applying molecular mechanics, normal mode analysis, molecular dynamics, and free energy calculations to simulate the structural and energetic properties of molecules. *Comp. Phys. Commun.* 91:1–41.

Perdew, J. P., K. Burke, and M. Ernzerhof. 1996. Generalized gradient approximation made simple. *Phys. Rev. Lett.* 77:3865–3868.

Perdew, J. P., K. Burke, and M. Ernzerhof. 1997. Generalized gradient approximation made simple. *Phys. Rev. Lett. E.* 78:1396.

Piana, S., and P. Carloni. 2000. Conformational flexibility of the catalytic Asp dyad in HIV-1 protease: an ab initio study on the free enzyme. *Proteins.* 39:26–36.

Polosukhina, K., D. Eden, M. Chinn, and S. Highsmith. 2000. CaATP as a substrate to investigate the myosin lever arm hypothesis of force generation. *Biophys. J.* 78:1474–1481.

Rothlisberger, U., P. Carloni, K. Doclo, and M. Parrinello. 2000. A comparative study of galactose oxidase and active site analogs based on QM/MM Car-Parrinello simulations. *J. Bio. Inorg. Chem.* 5:236–250.

Ryckaert, J. P., G. Ciccotti, and H. J. C. Berendsen. 1977. Numerical integration of Cartesian equations of motion of a system with constraints: molecular dynamics of n-alkanes. *J. Comput. Phys.* 23: 327–341.

Sablin, E. P., R. B. Case, S. C. Dai, C. L. Hart, A. Ruby, R. D. Vale, and R. J. Fletterick. 1998. Direction determination in the minus-end-directed kinesin motor ncd. *Nature.* 395:813–816.

Sablin, E. P., F. J. Kull, R. Cooke, R. D. Vale, and R. J. Fletterick. 1996. Crystal structure of the motor domain of the kinesin-related motor ncd. *Nature.* 380:555–559.

Sanner, M. F., A. J. Olson, and J. C. Spehner. 1996. Reduced surface—an efficient way to compute molecular species. *Biopolymers.* 38:302–320.

Sharp, K. A., and B. Honig. 1990. Electrostatic interactions in macromolecules—theory and applications. *Annu. Rev. Biophys. Biophys. Chem.* 19:301–332.

Smith, K. C., and B. Honig. 1994. Evaluation of the conformational free energies of loops in proteins. *Proteins.* 18:119–132.

Smith, C. A., and I. Rayment. 1996a. X-ray structure of the magnesium(II)-ADP-vanadate complex of the *Dictyostelium discoideum* myosin motor domain to 1.9 Angstrom resolution. *Biochemistry.* 35:5404–5417.

Smith, C. A., and I. Rayment. 1996b. Active site comparisons highlight structural similarities between myosin and other P-loop proteins. *Biophys. J.* 70:1590–1602.

Srinivasan, J., T. E. Cheatham III, P. Cieplak, P. A. Kollman, and D. A. Case. 1998. Continuum solvent studies of the stability of DNA, RNA, and phosphoramidate-DNA helices. *J. Am. Chem. Soc.* 120:9401–9409.

Sulpizi, M., and P. Carloni. 2000. Cation-π versus OH-π interactions in proteins: a density functional study. *J. Phys. Chem. B.* 104: 10087–10091.

Taylor, E. W. 1979. Mechanism of the actomyosin ATPase and the problem of muscle contraction. *Crit. Rev. Biochem.* 7:103–135.

Tuckerman, M. E., K. Laasonen, M. Sprik, and M. Parrinello. 1995. "Ab initio" molecular dynamics simulation of the solvation and transport of hydronium and hydroxyl ions in water. *J. Phys. Chem.* 99:5749–5752.

Vale, R. D. 1996. Switches, latches, and amplifiers: common themes of molecular motors. *J. Cell Biol.* 135:291–302.

Vanderbilt, D. 1990. Soft self-consistent pseudopotentials in a generalized eigenvalue problem. *Phys. Rev. B.* 41:7892–7985.

Walker, J. E., M. Saraste, M. J. Runswick, and N. J. Gay. 1982. Distantly related sequences in the a- and b-subunits of ATP synthase, myosin, kinases and other ATP-requiring enzymes and a common nucleotide binding fold. *EMBO J.* 1:945–951.

Wang, D., E. Pate, R. Cooke, and R. Yount. 1993. Synthesis of non-nucleotide ATP analogs and characterization of their chemomechanical interaction with muscle fibers. *J. Muscle Res. Cell Motil.* 14:484–497.

Yang, A. S., B. Hitz, and B. Honig. 1996. Free energy determinants of secondary structure formation. 3. Beta-turns and their role in protein folding. *J. Mol. Biol.* 259:873–882.

Yang, A. S., and B. Honig. 1995a. Free energy determinants of secondary structure formation. 1. Alpha-helices. *J. Mol. Biol.* 252:351–365.

Yang, A. S., and B. Honig. 1995b. Free energy determinants of secondary structure formation. 2. Antiparallel beta-sheets. *J. Mol. Biol.* 252: 366–376.

Yount, R. G., D. Lawson, and I. Rayment. 1995. Is myosin a "back door" enzyme? *Biophys. J.* 68:44S–47S.